Indian Journal of Pure & Applied Physics
Vol. 60, February 2022, pp. 126-130

Effect of Anatase and Rutile Phase Microspheres Composition on Dye-Sensitized Solar Cell Photoanode Performance

M Kandasamy[a,b], S Murugesan[a,*], Mohammed M Alam[c,*] & M Selvaraj[c]

[a]Department of Inorganic Chemistry, School of Chemistry, Madurai Kamaraj University, Madurai 625 021, India

[b]K. Ramakrishnan College of Technology, Samayapuram, Tiruchirappalli, Tamil Nadu 621 112, India

[c]Department of Chemistry, Faculty of Science, King Khalid University, Abha 61413, Saudi Arabia

Received 12 November 2021; accepted 17 January 2022

The effect of calcination temperature on the phase stability of solvothermally synthesized mesoporous anatase TiO_2 microspheres has been investigated through X-ray diffraction and Raman spectroscopy. Morphological change owing to anatase to rutile phase transformation has been examined by transmission electron microscopy. Dye-sensitized Solar Cell with anatase TiO_2 microspheres photoanode exhibits good photovoltaic performance with an overall cell efficiency of 4.47 %. Calcination above 900 °C reduces the efficiency. Incident Photon to Current Conversion Efficiency (IPCE) studies reveals that the TiO_2 microspheres calcined at 700 °C have high IPCE due to high dye loading owing to its high surface area and porous structure.

Keywords: Mesoporous TiO_2 microspheres, Nanocrystalline materials, Dye-sensitized solar cells; Phase transition; Solar energy materials.

1 Introduction

For the past 30 years, silicon solar cells hold the position as most popular solar cells in the world. In the recent years, dye-sensitized solar cells (DSSCs) are trying to replace the highly expensive silicon solar cells as DSSCs have the attractive features of relatively low fabrication costs, fairly good efficiency and flexible option[1–3]. The key component of DSSCs is the mesoporous TiO_2 nanocrystalline film on a conducting glass surface. Out of the three crystalline phase of TiO_2, namely anatase (tetragonal), rutile (tetragonal) and brookite (orthorhombic), anatase is preferred for DSSC[4-6]. The changes in morphology and crystalline phase of TiO_2 upon heat treatment from 600 to 1000 ºC was studied by Porter *et al.*[7] and reported an apparent increase of crystallite size, increase of rutile content and reduction of specific surface area with increasing calcination temperature. Similar effect was observed by Reddy *et al.*[8] for calcination in the range of 400 to 900 ºC wherein a decrease in lattice strain along with increase in crystallite size was noted above 600 ºC. While the photovoltaic performance of TiO_2 photoanode is highly relying on its crystallinity, morphology and crystalline phase[9–11], the anatase-rutile mixed phase perform well in general[12–15].

In this work, mesoporous anatase TiO_2 microspheres were synthesized solvothermally and performed XRD and Raman studies to examine its crystalline phase feature. The TiO_2 microspheres were calcinated at different temperatures *viz.,* 500, 700 and 900 °C in view of producing mixed phases. Prepared TiO_2 microspheres were integrated as photoanodes of DSSC and the influence of different phase compositions on photovoltaic performance was evaluated.

2 Experimental

2.1. Chemicals

Titanium(IV) isopropoxide or titaniumtetraiso propoxide (TIP, 97%), hexadecylamine (HDA, 90%) and N719 dye (di-tetrabutylammoniumcis-bis(isothiocyanato)bis(2,2′-bipyridyl-4,4′-dicarbo xylato) ruthenium(II)) were purchased from Sigma-Aldrich, India. Potassium chloride and ammonia solution (25%) were procured from Central Drug House (CDH), India. Double distilled water was used in all the experiments.

2.2. Synthesis of mesoporous TiO_2 microsphere

TiO_2 microspheres were synthesized *via* a modified reported procedure[16]. Accordingly, amorphous-TiO_2 microspheres were prepared first, through a simple sol-gel method, using 8.8 mL titaniumtetraiso propoxide, 0.22 M hexadecylamine (HDA) and 0.1 M

*Corresponding author:
(E-mail: murugesan.chem@mkuniversity.org; malm@kku.edu.sa)

KCl solution in 400 mL ethanol. To convert them into crystalline TiO_2 microspheres, 1 g of amorphous-TiO_2 microspheres were dispersed in a mixture of 20 mL ethanol and 10 mL water, followed by the addition of 1 mL ammonia solution. After an hour of ultrasonication, the mixture was transferred into an autoclave and heated at 160 °C (16 h). The product formed was washed with ethanol many times and dried (100 °C; 12 h). The so obtained product was calcined at various temperatures, *viz*., 500, 700 and 900 °C for 2 h and the corresponding products were denoted as MT500, MT700 and MT900, respectively.

2.3. Characterizations studies

Phase analysis of the prepared TiO_2 microspheres were examined by powder X-ray diffraction (XRD) technique (Rigaku diffractometer, CuKα radiation, λ= 1.5418 Å). The vibrational spectra of the prepared samples were recorded using Raman scattering (LabRam HR800, Horiba Jobin Yvon). The morphological analysis was performed using high-resolution transmission electron microscopy (HRTEM) with a FEI TECNAI-G^2 20 Twin instrument operated at 200 kV. The specific surface area of the various TiO_2 samples was determined in Quanta chrome 2200e *via* nitrogen adsorption studies at 77 K.

2.4. Fabrication and testing of DSSCs

Fluorine doped tin oxide (FTO) glass substrates were immersed in $TiCl_4$ solution (40 mM) for 30 min at 70 °C and washed using water and ethanol, and then annealed at 420 °C for 30 min. The TiO_2 photoanode films were fabricated by a standard doctor-blade method[1], and subsequently calcined at 450 °C for 20 min. After sintering process, the photoanodes were naturally cooled down to 80 ºC and the photoanodes were immersed in N719 dye for 24 h. The platinum (Pt) coated counter electrodes were prepared by thermal decomposition of H_2PtCl_6 at 420 °C for 20 min. The DSSCs were assembled using TiO_2 photoanode, Pt counter electrode and the liquid electrolyte. The active area of the cell was 1 × 1 cm^2. The current density-voltage (J–V) measurements were performed at AM1.5G illumination (85 mW cm^{-2}) from a solar simulator. Incident photon to current conversion efficiency (IPCE) characteristics were measured with an Enlitech QE-T spectral response measurement system.

3 Results and Discussion

3.1. Raman and XRD analyses

Fig. 1 displays the XRD patterns and Raman spectra of the newly prepared TiO_2 microsphere samples

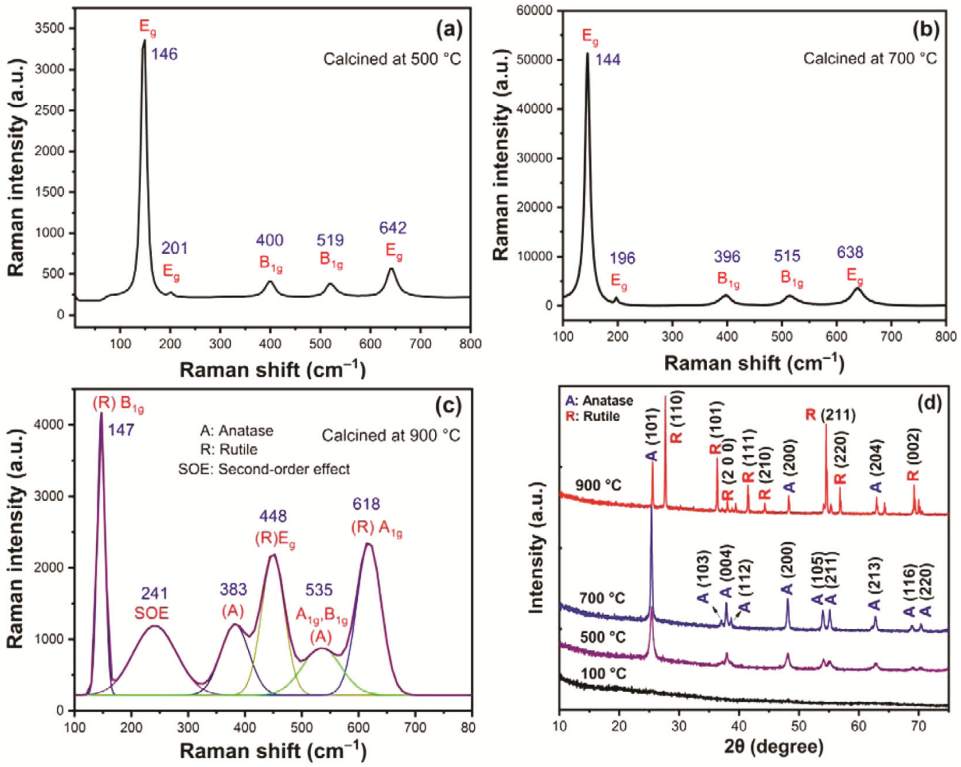

Fig. 1 — Raman spectra (a-c) and XRD patterns (d) of the prepared TiO_2 microsphere samples.

calcined at various temperatures. Both MT500 and MT700 samples show five vibrational bands assignable to E_g (144, 196 and 638 cm^{-1}) and B_{1g} (396 and 515 cm^{-1}) symmetry species of anatase TiO_2[17]. However, MT700 sample (annealed at 700 °C) show very high intensity peaks compared to MT500 indicating that the MT700 sample has high crystallity anatase phase. As shown in Fig. 1(c), the MT900 sample shows prominent vibrational bands at 147, 448, and 618 cm^{-1}, respectively assigned to the B_{1g}, E_g and A_{1g} symmetry species of rutile. That is, increasing the calcination temperature to 900 °C brings profound changes in the Raman spectrum of TiO_2 attributable to anatase to rutile phase transformation. The broad band at 241 cm^{-1} can be attributed to second-order or two-phonon Raman scattering[18]. Although barely discernible in the Raman spectrum of MT900, there was a very weak lattice vibrational band at 828 cm^{-1} (not shown) corresponding to the B_{2g} symmetry species of rutile. It reveals a clear progress of phase transformation from anatase to rutile phase.

From the XRD patterns it can be seen that the as-prepared material is amorphous. The XRD patterns of MT500 and MT700 exhibit diffraction peaks at 2θ values of 25.2, 37.7, 48.02, 53.8, 55.1, 62.6, 68.8 and 70.3° assigned to (101), (004), (200), (105), (211), (213), (116) and (220) planes of anatase phase which is in good agreement with standard JCPDS file No. 21-1272. It reveals that calcination upto 700 °C leads to formation of purely anatase TiO_2. Upon increasing the annealing temperature from 500 to 700 °C, the (101) peak of anatase becomes sharper and stronger. This is because; the original bonds in the amorphous particles broke to form new bonds of anatase structure during high temperature crystallization process, resulting in the deformation of particles and the formation of crystals[19–21]. For the sample calcined at 900 °C, the XRD pattern Fig. 1(d) consists primarily of sharp peaks of rutile phase, *viz*., peaks at 2θ values of 27.6, 34.4, 41.4, 56.8 and 69.1° indexed to (110), (101), (111), (211) and (301) planes of rutile phase (JSPDS file No. 21-1276), with concomitant disappearance of anatase peaks. The relative abundance of the anatase and rutile phases were calculated using the Spurr's formula[22]: $W_R = 1.26I_R / I_A+1.26I_R$, where W_R is fraction of rutile phase, I_R and I_A are maximum intensities of rutile (110) and anatase (101) diffraction peaks, respectively. The rutile content in MT900 was found to be 72%. This means, even at 900 °C the phase transformation is not complete[23]. The sample calcined at 900 °C contains mixture of anatase and rutile phases, and their crystallite size increases significantly after the phase transformation from anatase to rutile. The average crystallite sizes of the prepared TiO_2 microspheres calculated using Scherrer's equation[24] are found to be 17.2, 24.5 and 55.7 nm, respectively for the MT500, MT700 and MT900 samples.

3.2. HRTEM analysis

Fig. 2 shows the HRTEM images and SAED patterns of TiO_2 microspheres heat-treated at 700 and 900 °C. The morphology has significantly changed upon increasing the calcination temperature from 700 to 900 °C. The TiO_2 microspheres calcined at 700 °C Fig. 2(A1) contain microspheres (500-600 nm) composed of spherical nanoparticles (20 nm), which is caused by the initial formation of crystalline anatase. Upon further increasing the calcination temperature to 900 °C Fig. 2(B1), the TiO_2 particles are merged to form the disc shaped rutile crystallites, which may be attributed to the increase of internal stress with the shrinkage of the TiO_2 on anatase to rutile transformation. Moreover, high-temperature annealing would reduce the overall surface area. From HRTEM

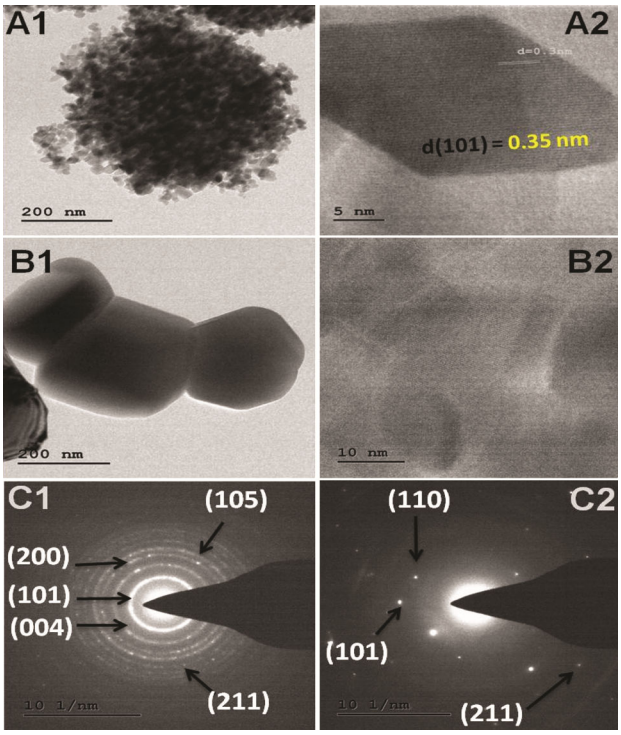

Fig. 2 — (A1&A2): TEM images of MT700 and MT900; (B1&B2) HRTEM images of MT700 and MT900; and (C1&C2) SAED patterns of MT700 and MT900.

images Fig. 2(A2&B2), the presence of crystalline nanoparticles of anatase and rutile are confirmed. The selected area electron diffraction (SAED) patterns Fig. 2(C1&C2), further confirms the anatase and rutile phases in the MT700 and MT900 respectively.

3. 3. Photovoltaic performance of DSSC

Photocurrent density versus photovoltage (J-V) curves of the DSSCs made of photoanodes with TiO_2 microspheres calcined at various temperatures (MT500, MT700 and MT900) are shown in Fig. 3(a) and the corresponding photovoltaic parameters are listed in Table 1. The photocurrent density (9.23 mA cm^{-2}) of the TiO_2 microspheres calcined at 700 °C is higher than that of photoanodes with MT500 (8.49 mA cm^{-2}). Consequently, as seen in Table 1, DSSC with MT700 based photoanode exhibits high conversion efficiency (η) of 4.47%. Interestingly, the device based on MT900 photoanode show lower conversion efficiency (2.07%) than the device with MT700 based photoanode (4.47%). The high efficiency of MT700 is attributed to its high crystallinity with high surface area (32.2 m^2 g^{-1}), which facilitates high dye loading. In the TiO_2 microspheres, the chemical connection between the TiO_2 nanoparticles is improved, thereby providing enhanced electron diffusion in the film. This also helps in improving the penetration of liquid electrolyte. As a consequence, the charge recombination is effectively reduced and thus the J_{sc} is enhanced.

The MT900 photoanode showed relatively low photoconversion efficiency due to its high rutile content (72%). The MT900 with relatively larger rutile crystallites has lower dye loading capability owing to their large particle size and lower surface area[25, 26]. It is known that the anatase TiO_2 is more favourable for photoanode in DSSCs due to the favourable flat-band potential of anatase in comparison to rutile. The anatase TiO_2 conduction band is 0.2 V more negative than that of rutile TiO_2, so high photovoltage can be obtained on anatase (MT700) than rutile (MT900) in the same redox mediator[25, 27].

The IPCE spectra Fig. 3(b) also in-line with the observed trend, *i.e.*, MT900 show lower IPCE than MT700. It can be seen that there is a large difference of IPCE spectra at longer wavelengths (>500 nm), which indicates that a much smaller amount of dye is contained in MT900 sample. As a result, electron transport is less in the rutile phase of TiO_2 film than in the anatase TiO_2[28–30]. The enhanced IPCE at 500-550 nm wavelengths for MT700 can be credited to higher dye loading. Thus, the high IPCE of the DSSC fabricated with the MT700 photoanode results in a high photocurrent density and photovoltaic performance.

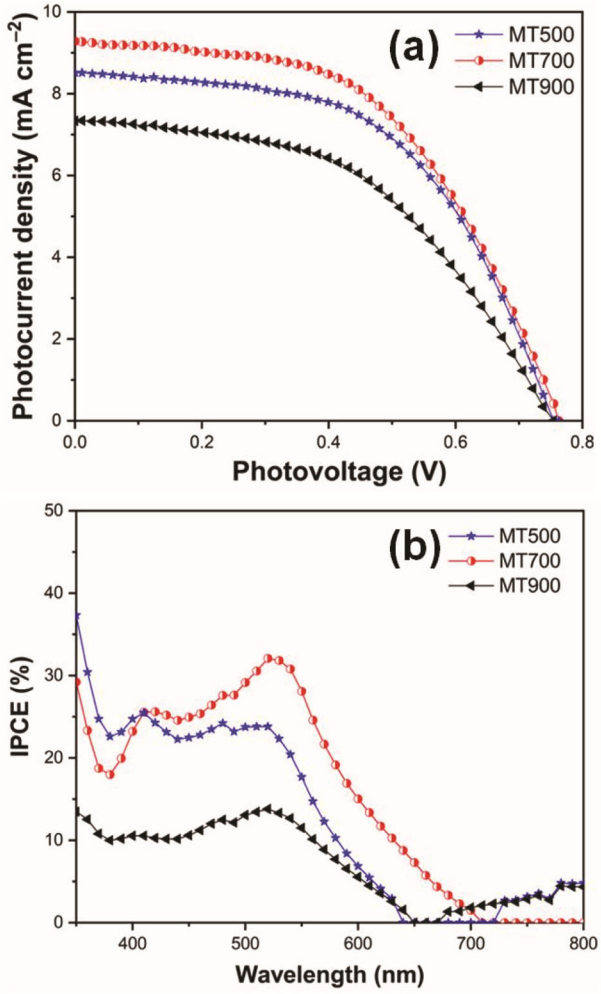

Fig. 3 — (a) Photocurrent density-voltage (*J-V*) characteristics and (b) IPCE spectra of the DSSC based on the prepared TiO_2 microspheres. Cell area = 1 × 1 cm^2.

Table – 1 — Photovoltaic parameters of dye-sensitized solar cells with different TiO_2 photoanodes[a]

Photoanode	J_{SC} (mA cm^{-2})	V_{OC} (V)	FF	η (%)	$IPCE_{max}$ (%)
MT500	8.49	0.755	0.43	3.23	22
MT700	9.29	0.761	0.53	4.47	32
MT900	4.12	0.722	0.59	2.07	13

4. Conclusions

Anatase to rutile phase transformation of the prepared TiO_2 microspheres has occurred gradually

upon heat treatment in the range of 700 to 900 °C. About 72% of anatase phase is changed to rutile phase at 900 °C. Study of dye-sensitized solar cells integrated with anatase TiO_2 microspheres or rutile TiO_2 microspheres demonstrates that the DSSC with MT700 photoanode (TiO_2 calcined at 700 °C) exhibited superior photovoltaic conversion efficiency (η) of 4.47% compared to the MT900 photoanode device (2.07%). The better photovoltaic performance associated with MT700 photoanode can be attributed to the increased surface area (32.2 $m^2\ g^{-1}$), higher dye loading and favourable anatase phase for electron transfer which reduced the recombination of electrons and holes.

Acknowledgements

UGC, India and DST-Government of India are acknowledged for providing instrumental facilities through UGC-UPE and DST-PURSE Schemes. M.M. Alam and M. Selvaraj thank KKU, Saudi Arabia for funding by way of a research group project (R.G.P. 1/356/1442).

References

1 Nazeeruddin M K, Kay A, Rodicio I, Humphry-Baker R, Muller E, Liska P, Vlachopoulos N & Gratzel M, *J Am Chem Soc*, 115 (1993) 6382.
2 Bernardi M & Grossman J C, *Energy Environ Sci*, 9 (2016) 2197.
3 Muchuweni E, Martincigh B S & Nyamori V O, *RSC Adv*, 10 (2020) 44453.
4 Li J G, Ishigaki T, & Sun X, *J Phys Chem C*, 111 (2007) 4969.
5 Hossain M K, Mortuza A A, Sen S K, Basher M K, Ashraf M W, Tayyaba S, Mia M N H & Uddin M J, *Optik*, 171 (2018) 507.
6 Ismail M, Chebaane M M, Bousselmi L, Zahraa O, Olivier C & Toupance T, *Surf Interfaces*, 27 (2021) 101543.
7 Porter J F, Li Y, & Cahn C K, *J Mater Sci*, 34 (1999) 1523.
8 Reddy K M, Reddy C V G & Manorama S V, *J Solid State Chem*, 158 (2001) 180−186.
9 Ohno T, Sarukawa K, Tokieda K & Matsumura M, *J Catal*, 203 (2001) 82.
10 Estruga M, Domingo C, Domenech X & Ayllon J A, *Nanotechnology*, 20 (2009) 125604.
11 Liu Z, Zhang X, Nishimoto S, Jin M, Tryk D A, Murakami T & Fujishima A, *Langmuir*, 23 (2007) 10916.
12 Guimarães R R, Parussulo A L A, Toma H E & Araki K, *Electrochim Acta*, 188 (2016) 523.
13 Suriani A B, Muqoyyanah, Mohamed A, Mamat M H, Hashim N, Isa I M, Malek M F, Kairi M I, Mohamed A R & Ahmad M K, *Optik*, 158 (2018) 522.
14 Shahid M U, Mohamed N M, Muhsan A S, Zaine S N A, Bashiri R, Khatani M & Samsudin A E, *Sol Energy*, 206 (2020) 317.
15 Wu Y H, Yuan K Y, He Y E, Wu H, Ma L J, Wang G, Qiao X D, Lei B X, Sun Z F & Liu Z Q, *Chin Chem Lett*, (In Press)
16 Chen D, Huang F, Cheng Y B & Caruso R A, *Adv Mater*, 21 (2009) 2206.
17 Tompsett G A, Bowmaker G A, Cooney R P, Metson J B, Rodgers K A & Seakins J M, *J Raman Spectroscopy*, 26 (1995) 57.
18 Zhang J, Xu Q, Li M, Feng Z & Li C, *J Phys Chem* C, 113 (2009) 1698.
19 Beams R, Cancado L G & Novotny L, *J Phys: Condens Matter*, 27 (2015) 083002.
20 Kashyout A B, Soliman M & Fathy M, *Renewable Energy*, 35 (2010) 2914.
21 Yu H K, Eun T H, Yi G R & Yang S M, *J Colloid Interface Sci*, 316 (2007) 175.
22 Spurr R A & Myers H, *Anal Chem*, 29 (1957) 760.
23 Penn R L & Banfield J F, *Am Mineral*, 84 (1999) 871.
24 Scherrer P, *Göttinger Nachrichten Math Phys*, 2 (1918) 98.
25 Yun T K, Park S S, Kim D, Shim J-H, Bae J Y, Huhc S, & Won Y S, *Dalton Trans*, 41 (2012) 1284.
26 Wategaonkar S B, Pawar R P, Parale V G, Nade D P, Sargar B M & Mane R K, *Mater Today Proc*, 23 (2020) 444.
27 Cahen D, Hodes G, Gratzel M, Guillemoles J F & Riess I, *J Phys Chem B*, 104 (2000) 2053.
28 Kavan L, Grätzel M, Gilbert S E, Klemenz C & Scheel H J, *J Am Chem Soc*, 118 (1996) 6716.
29 Lee K M, Suryanarayanan V & Ho K C, *Sol Energy Mater Sol Cells*, 91 (2007) 1416.
30 Shaikh S F, Mane R S, Min B K, Hwang Y J & Joo O, *Sci Reports*, 6 (2016) 20103.